Welding of Gold Nanoparticles on Graphitic Templates for Chemical Sensing

Mengning Ding,[†,‡] Dan C. Sorescu,[†] Gregg P. Kotchey,[‡] and Alexander Star*[,†,‡]

[†]National Energy Technology Laboratory, U.S. Department of Energy, Pittsburgh, Pennsylvania 15236, United States
[‡]Department of Chemistry, University of Pittsburgh, Pittsburgh, Pennsylvania 15260, United States

S *Supporting Information*

ABSTRACT: Controlled self-assembly of zero-dimensional gold nanoparticles and construction of complex gold nanostructures from these building blocks could significantly extend their applications in many fields. Carbon nanotubes are one of the most promising inorganic templates for this strategy because of their unique physical, chemical, and mechanical properties, which translate into numerous potential applications. Here we report the bottom-up synthesis of gold nanowires in aqueous solution through self-assembly of gold nanoparticles on single-walled carbon nanotubes followed by thermal-heating-induced nanowelding. We investigate the mechanism of this process by exploring different graphitic templates. The experimental work is assisted by computational studies that provide additional insight into the self-assembly and nanowelding mechanism. We also demonstrate the chemical sensitivity of the nanomaterial to parts-per-billion concentrations of hydrogen sulfide with potential applications in industrial safety and personal healthcare.

INTRODUCTION

The bottom-up synthesis of complex architectures from nanoscale building blocks is a fascinating approach to achieve novel materials with unique structures and functions; yet this process remains extremely challenging because it requires careful and delicate control of the building blocks at a molecular level.[1−3] One representative example involves the fabrication of one-dimensional (1-D) gold nanowires (AuNWs) from zero-dimensional (0-D) gold nanoparticles (AuNPs), which have been extensively studied due to their potential applications in electronics,[4,5] photonics,[6] and sensors.[7] The difficulty with this system arises from the need to precisely place and interconnect individual NPs in a confined dimension.[8,9] Successful bottom-up fabrication of AuNWs has been accomplished through an "oriented attachment" method,[10−12] where recognition of the anisotropic lattice and the reduction of surface energy played essential roles.[13,14] The welding of gold at the nanoscale was another approach for the bottom-up construction of gold nanostructures. Since this method does not require the templating of strong binding surfactants such as oleylamine, it is favorable for the fabrication of catalysts and chemical sensors. The welding of gold nanostructures has been successfully implemented by a number of methods such as laser heating,[15] Joule heating,[16] and cold welding.[17] Combining nanowelding with self-assembly of AuNPs provides another promising bottom-up strategy for the fabrication of AuNWs from AuNPs; one example of such a strategy has been successfully demonstrated by Belcher and co-workers utilizing biological templates.[18]

Progress made on controlled fabrication of Au nanostructures will significantly benefit the development of chemical sensors. Au has been used in chemical sensors for decades[19] because of its chemical inertness and high conductivity, which changes upon adsorption of different molecules. Hydrogen sulfide (H_2S), for example, has been detected using Au thin films,[20] AuNPs,[21] and most recently AuNPs-decorated carbon nanotubes (CNTs).[22,23] Despite the excellent sensitivity achieved by AuNPs for H_2S, there has been minimal advance in the development of H_2S sensors based on AuNWs. 1-D nanostructures have been considered to be an ideal sensor architecture because their Debye length is comparable to the cross-sectional radius;[24,25] therefore, it is of great interest to explore the H_2S sensitivity of 1-D AuNWs.

Here we report a bottom-up approach for the synthesis of AuNWs using AuNPs as building blocks in aqueous suspensions of single-walled carbon nanotubes (SWNTs). Citrate-stabilized AuNPs first underwent a 1-D self-assembly process enabled by 1-pyrenesulfonic acid (PSA)-decorated SWNT templates, and AuNWs were subsequently formed through a nanowelding process of aligned AuNPs induced by thermal heating. In addition to performing control experiments with different graphitic templates, we used density functional theory (DFT) calculations to understand the underlying mechanism of the entire self-assembly and nanowelding processes. We further demonstrated the use of AuNW-SWNTs hybrid material for sensitive and selective detection of H_2S gas. We established that, with its ultrasensitivity to H_2S at concentrations as low as parts-per-billion (ppb) and no obvious cross-sensitivity toward major components of natural
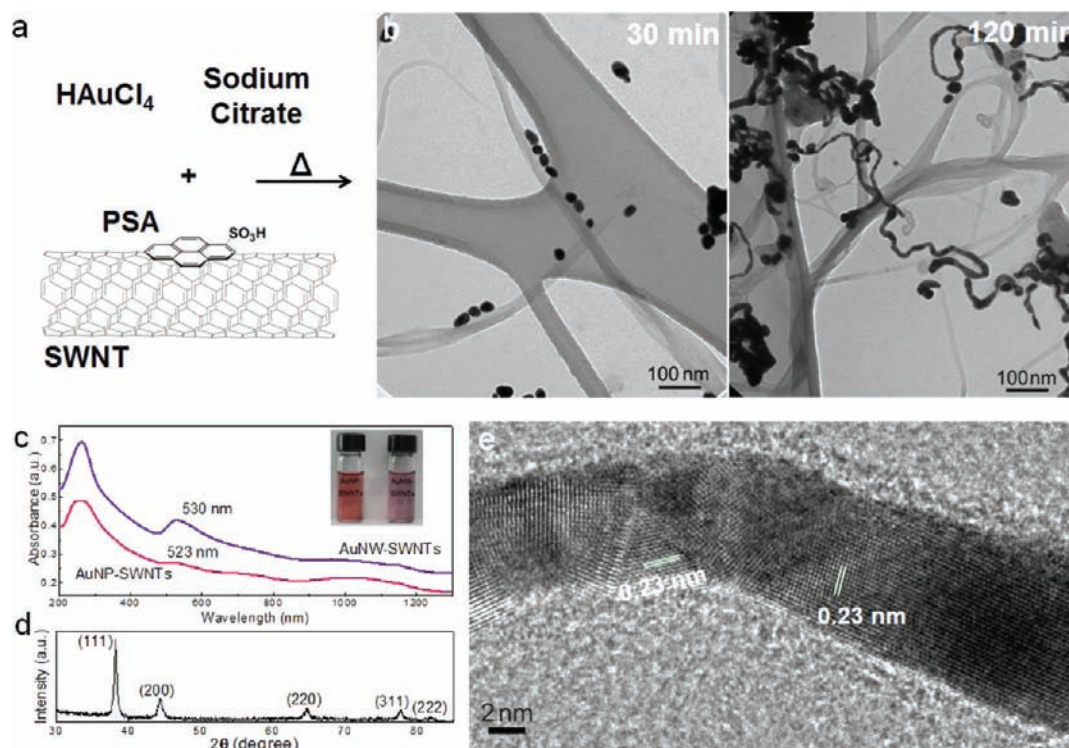
Figure 1. Synthesis and characterization of gold nanowires. (a) An aqueous suspension of 1-pyrenesulfonic acid (PSA)-functionalized single-walled carbon nanotubes (SWNTs) was used as a template during citrate reduction of HAuCl$_4$. (b) TEM images showing the assembly of AuNPs on the SWNTs (after 30 min, left) and their welding into AuNWs (after 120 min, right). (c) UV−vis−NIR absorption spectra of AuNW-SWNTs and AuNP-SWNTs samples. Gold surface plasmon resonance shows a red shift with increasing size of gold nanostructures. The inset depicts a digital photo of vials containing suspensions of AuNPs and AuNWs (with SWNTs). (d) X-ray diffraction pattern of AuNWs. (e) High-resolution TEM image of AuNWs showing the polycrystalline nature of the welded AuNWs.

gas and human breath, this material has potential applications in industrial sensors for personal safety and human breath detection.

■ RESULTS AND DISCUSSION

Bottom-Up Synthesis of AuNW-SWNTs. The formation, assembly, and welding of AuNPs were first carried out by an *in situ* citrate reduction of chloroauric acid (HAuCl$_4$) in a suspension of SWNTs, as illustrated in Figure 1a. SWNTs were first functionalized with PSA to form a uniform aqueous suspension[26] in which HAuCl$_4$ was later dissolved. The reduction of HAuCl$_4$ was started by the addition of sodium citrate solution, and the reaction proceeded at a controlled temperature (100 °C) with vigorous stirring.

Transmission electron microscopy (TEM) images (Figure 1b) showed the self-assembly of AuNPs on the sidewall of functionalized SWNTs 30 min after initialization of the reaction. Some NPs already appeared in an elongated shape, and the interconnections between NPs started to form. Both of these results indicated that the AuNPs started to fuse together under the reaction temperature. This fusion occurred regardless of the presence of SWNTs and could be understood as a nanowelding process of aggregated NPs induced by thermal heating.[27] After a longer reaction time, the nanowelding process resulted in the complete formation of NWs. The final solution appeared purple in color due to a red shift in the Au surface plasmon resonance from AuNPs to AuNWs (Figure 1c), which was in accordance with the optical studies on other 1-D Au nanostructures.[16] The X-ray diffraction pattern of AuNWs corresponded to a face-center cubic (fcc) structure (Figure 1d).

The fcc structure was also confirmed by high-resolution TEM (HRTEM), as shown in Figure 1e, where the interfringe distances of AuNW lattice were measured to be 0.23 nm, in agreement with (111) lattice spacing for fcc gold.

Compared with AuNWs that were prepared from confined growth of Au nanocrystals,[4] this self-assembly and nanowelding approach produced curved and flexible AuNWs. As can be observed from HRTEM, these AuNWs also exhibited different crystalline areas, which indicated that the NWs were constructed from multiple building blocks and the assembly was not directed by lattice match as in the case of "oriented attachment".[10−12] This was further confirmed by the HRTEM interfringe patterns observed on a single AuNP and on an early stage wire that consisted of a few AuNPs welded together (Figure S1, Supporting Information). In addition, small portions of AuNWs also exhibited a single-crystalline composition, as shown in Figure 1e (right part of the NW, also see Figure S2). Since the welded NPs were initially polycrystalline in nature, the observation of a single-crystalline segment indicated a potential alternation of the crystallinity of these AuNWs. Similar programmable assembly and growth of Au nanoarchitectures was reported for biological templates (genetically engineered viruses).[18] Our results demonstrated that inorganic templates such as SWNT-PSA or MWNT-PSA (Figure S3) complexes can be employed in such a bottom-up strategy.

Assembly and Nanowelding of AuNPs on Other Graphitic Templates. In control experiments, HAuCl$_4$ solution was reduced under similar synthetic conditions (−SWNTs, −PSA or +PSA), and representative TEM images
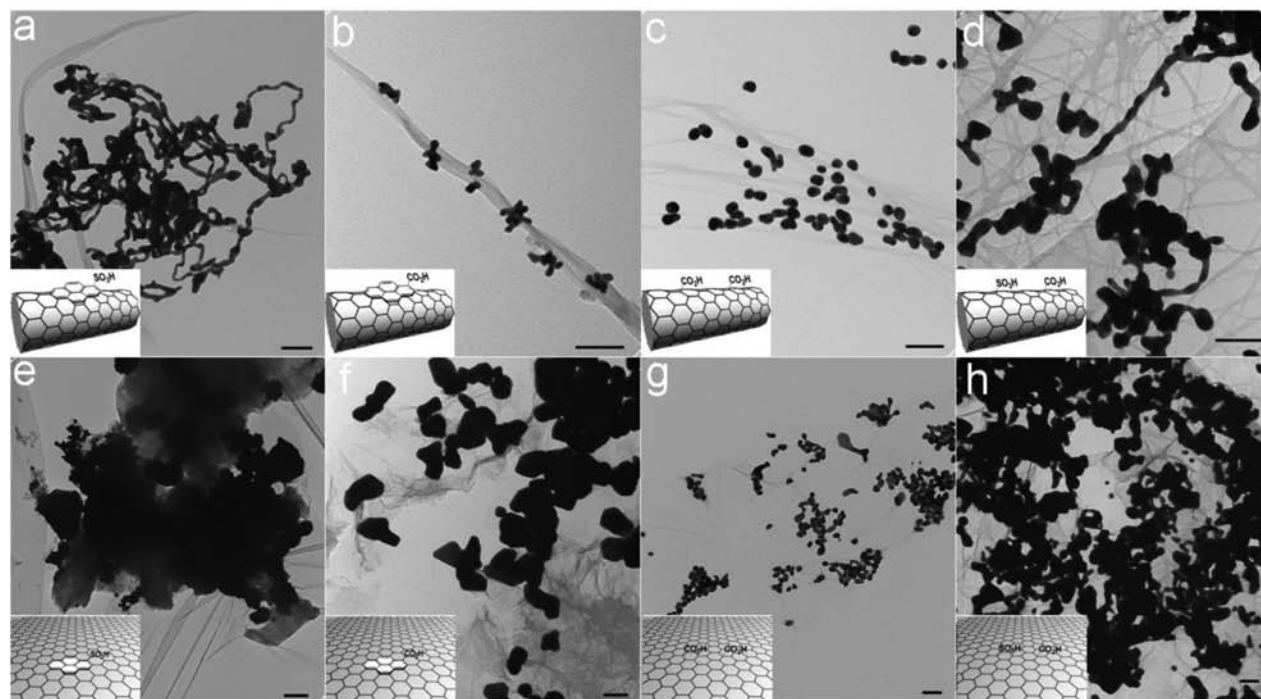
Figure 2. TEM images of the products after AuNPs assembly and nanowelding using different graphitic templates. (a) PSA-functionalized SWNTs (SWNT-PSA). (b) 1-Pyrenecarboxylic acid (PCA)-functionalized SWNTs (SWNT-PCA). (c) Carboxylated SWNTs (SWNT-COOH). (d) Sulfonated SWNTs (S-SWNTs). (e) PSA-functionalized chemically converted graphene (CCG-PSA). (f) PCA-functionalized chemically converted graphene (CCG-PCA). (g) Graphene oxide (GO). (h) Sulfonated chemically converted graphene (S-CCG). Scale bars in (a–d) and (f–h) are 100 nm; scale bar in (e) is 500 nm. Insets are cartoon presentations of the surface functionalizations of the templates.

of the products are shown in Figure S4. Without SWNTs in the reaction mixture, AuNWs were not observed regardless of PSA concentration; only aggregates of AuNPs were present (with some of them already fused together).

This observation indicated the necessity of utilizing SWNT templates for the formation of NW structures. Furthermore, in another control experiment, commercially available gold colloidal solution (Sigma Aldrich) was used as the prefabricated building blocks with the SWNT-PSA template; both self-assembly of the NPs and the nanowelding process were observed (Figure S5). This result clearly demonstrated that the self-assembly and nanowelding processes do not require *in situ* synthesis of the AuNPs in the system and can be utilized as a general bottom-up approach for the synthesis of 1-D nanomaterials. Our methodology also permitted the successful synthesis of other 1-D nanostructures such as platinum NWs (Figure S6).

The entire self-assembly process, which included adsorption and in-plane diffusion of NPs, was significantly affected by the surface chemistry of both NPs and templates. In order to elucidate such effects, the AuNPs assembly and nanowelding processes were conducted on other graphitic templates, including 1-pyrenecarboxylic acid (PCA) functionalized SWNTs (SWNT-PCA), carboxylated SWNTs (SWNT-COOH, P3, Carbon Solutions, Inc.), and sulfonated SWNTs (S-SWNT), as well as 2-D templates, including PSA- and PCA-functionalized chemically converted graphene (CCG-PSA/CCG-PCA), graphene oxide (GO), and sulfonated chemically converted graphene (S-CCG). By choosing this set of templates, we were adept at exploring the effects of template surface functionalities on the diffusion of AuNPs, which in turn enhanced our understanding of the assembly process.

Although 1-D AuNWs were formed with SWNT-PSA (Figure 2a), different products were observed with other templates (Figures 2b–h). When SWNT-PCA was employed as the template, small aggregates of several NPs were observed after the welding process instead of NWs, as shown in Figure 2b. Although PCA and PSA molecules share a pyrene functionality that is capable of $\pi-\pi$ stacking interactions with graphitic surfaces,[28] the presence of carboxylic groups (−COOH) as opposed to sulfonic groups (−SO_3H) appears to have prevented the formation of AuNWs. We further probed SWNT-COOH as templates, which have a high degree of carboxylic functionalities, in order to confirm the effect of carboxylic functional groups. Similar to PCA case, only NPs that were attached to the nanotubes were observed (Figure 2c).

To further confirm the proposed influence of surface functional groups on the assembly process, S-SWNTs were explored as another template. This material was synthesized through the sulfonation of oxidized SWNTs with an aryl diazonium salt of sulfanilic acid followed by a hydrazine reduction, following a published procedure.[29] S-SWNTs contained both sulfonic and carboxylic groups and had a high solubility in water.[30] As shown in Figure 2d, S-SWNT templates led to the formation of an intermediate level product that possessed a few NWs; most products, however, were aggregated particles. The assembly and welding processes of AuNPs were further explored on 2-D graphene templates. As shown in Figure 2e–h, products from CCG-PSA, CCG-PCA, GO, and S-CCG followed the same trends as those observed for SWNTs. CCG-PSA resulted in full coverage on the graphene after nanowelding (as shown in Figure 2e). A number of small gold plates were formed in several confined areas on CCG-PCA (Figure 2f) after the welding of small
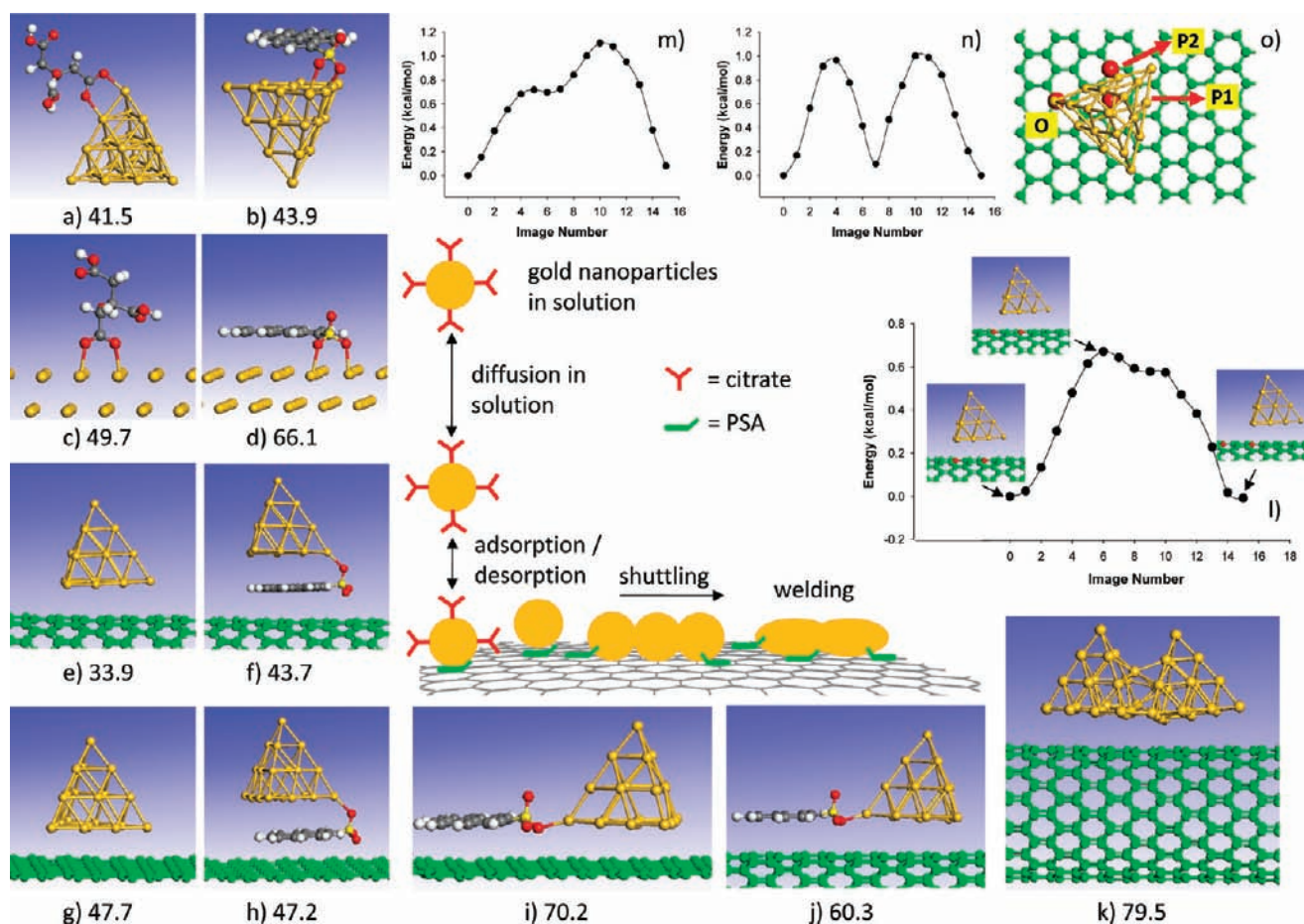
Figure 3. Molecular modeling of the adsorption, assembly, and nanowelding processes. The middle panel represents a schematic description of the adsorption, diffusion and welding mechanistic steps involved in the formation of AuNWs from Au clusters on CNT (graphene) surfaces decorated with PSA molecules. The indicated panels correspond as follows: adsorption configurations of citrate and PSA systems on a Au_{20} cluster (a,b) and on Au(111) surface (c,d), respectively; adsorption configurations of a Au_{20} cluster on a bare and PSA decorated CNT (e,f,j) and on bare and PSA-decorated graphene (g,h,i); and the welding of two Au_{20} clusters on CNT surface (k). Panel l represents the minimum energy pathway for diffusion of an Au_{20} cluster on a CNT surface in an axial direction between two surface sites marked in red. Panels m and n represent the minimum energy diffusion pathways of the Au_{20} cluster on graphene surface starting from an initial position O and taken along two different directions P1 and P2, indicated by red arrows in panel o. The indicated atomistic configurations correspond to the most stable states identified based on dispersion-corrected DFT calculations. In each case the corresponding binding energies (in kcal/mol) are given with respect to the isolated adsorbate and surface subsystems. In panels a–d the adsorption energies of citrate and PSA ions are indicated, while in panels e–k the adsorption energies of the Au_{20} cluster are shown. For PSA and citrate systems the C atoms are represented in gray, O atoms in red, H atom in white, and S atom in yellow; for graphene and CNT surfaces the C atoms are shown in green, while the Au atoms are represented in orange.

AuNPs aggregates. Furthermore, while free NPs were observed for GO templates (Figure 2g), an intermediate network of Au nanostructures (Figure 2h) was formed using S-CCG as templates.

Mechanism and Theoretical Simulations of the Assembly and Nanowelding Processes. Computational simulations were employed to provide a mechanistic understanding of the self-assembly and nanowelding processes and to rationalize the observed trends of different templates. The proposed self-assembly and nanowelding processes of AuNPs that consists of three mechanistic steps are detailed in Figure 3. In the first step, the AuNPs that formed in the solution phase and were functionalized with citrate molecules adsorbed onto the surface of SWNTs or graphene. In the second step, the adsorbed AuNPs can diffuse on the corresponding graphitic surfaces, and upon meeting, the AuNPs will nanoweld (third mechanistic step). The net result of these steps renders AuNPs as either 1-D NWs on the surfaces of SWNTs or as 2-D islands on graphene surfaces.

Specific details in support of these mechanistic steps are provided in Figure 3. In panels a–d, we present the most stable adsorption configurations of citrate and PSA anion on small (Au_{20}) clusters and on extended Au(111) surfaces. In both cases, there were appreciable interaction energies, but PSA demonstrated increased stability relative to citrate that could be correlated to the bonding type observed for these two systems. In the case of the citrate ion, adsorption took place exclusively through formation of CO-Au bonds (Figure 3a,c); for PSA, both the SO—Au bonds and the long-range dispersion interactions between the aromatic carbon rings and the Au surface (Figure 3b,d) contributed to the increased stability. These dispersion interactions between AuNPs and aromatic carbon structures have been recognized in other recent studies[31,32] and were also believed to provide partial support for the strong binding between AuNPs and peptides with aromatic residues.[33,34] Similar dispersion interactions were found to be responsible for the adsorption of Au_{20} NPs on pristine SWNT (Figure 3e) or on graphene (Figure 3g)
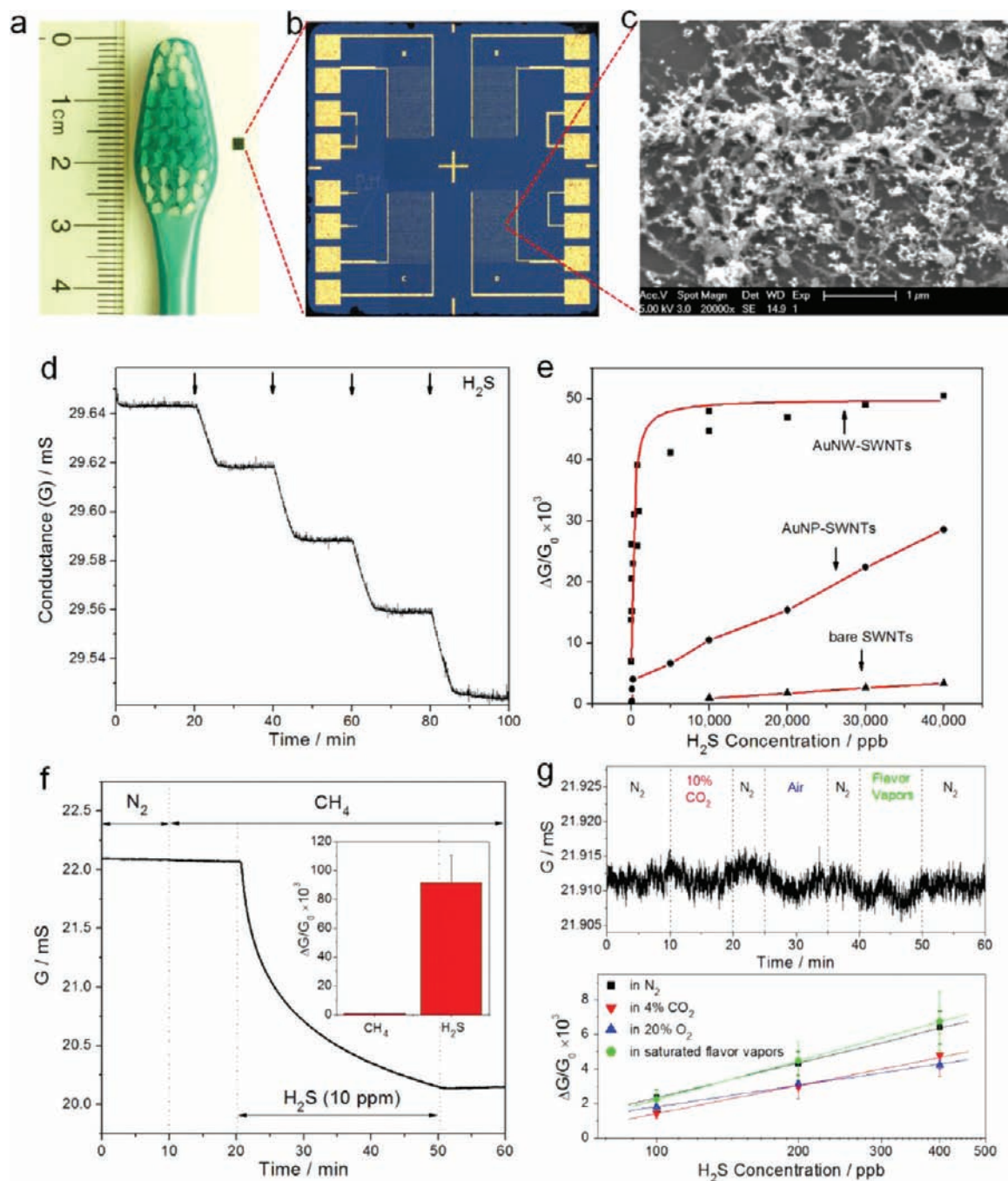
Figure 4. Hydrogen sulfide sensitivity of AuNW-SWNT devices. (a) A photograph of the chemiresistor chip in comparison to a toothbrush. (b) An optical image of the chip with micropatterned four interdigitated gold electrodes. (c) SEM image of the AuNW-SWNTs hybrids network bridging two fingers of interdigitated electrodes. (d) A typical real-time network conductance measurement in pure nitrogen and upon four H_2S exposures (5 min) with concentrations of 100 ppb, 200 ppb, 400 ppb, and 1 ppm; arrows correspond to the points when H_2S gas was introduced. (e) Electrical response of AuNW-SWNT, AuNP-SWNT, and bare SWNT networks to various concentrations of H_2S gas (5 min). The relative conductance change ($\Delta G/G_0$) of AuNW-SWNTs fits the Langmuir isotherm (red curve). (f) Cross-sensitivity of AuNW-SWNTs to typical natural gas components (methane); inset depicts the comparison of the sensor response to 100% methane and 10 ppm H_2S in methane. (g) Cross-sensitivity of AuNW-SWNTs to typical human breath components (carbon dioxide, oxygen, and flavor vapors); top depicts the response of AuNW-SWNTs to 10% carbon dioxide, 20% oxygen (air), and saturated vapors of commercial flavor mixture from Colgate-Palmolive Co., and bottom depicts the sensor response to H_2S (5 min) with concentrations of 100 ppb, 200 ppb, and 400 ppb in nitrogen, 4% carbon dioxide, 20% oxygen, and saturated vapors of flavor mixture.

surfaces. In the case of PSA-functionalized graphitic surfaces, Au_{20} clusters could adsorb either on top of the PSA molecule (Figure 3f,h) or directly on the graphitic surface with simultaneous binding to PSA (Figure 3i,j). The increased stability observed for these latest configurations was a consequence of the fact that Au_{20} cluster interacts simultaneously with SWNT (graphene) surfaces through dispersion interactions as well as through formation of SO−Au bonds to PSA molecules. In the case of larger AuNPs, it was expected that PSA molecules would decorate the NPs, particularly in the

interface region with graphitic surface. These results provided valid support for the first adsorption step in our proposed mechanism, where PSA on the surface of SWNTs replaced the citrate to bind AuNPs when SWNT-PSA/CCG-PSA were used as templates.

Additionally, other adsorption configurations were simulated to rationalize the synthetic results obtained when using different graphitic templates. For the SWNT-PCA system, comparable interaction energies were found for the adsorption of PCA anion on Au_{20} and Au(111) surfaces (Figure S7a,e and b,f), which did not match the different results observed in the synthesis. However, the dissociation of pyrene acid in the aqueous system was a factor that should be considered in this case. Unlike the strong acid PSA (with $pK_a \approx 0.7$),[35] PCA is a weak acid with $pK_a = 4.0$ that mostly remained in a neutral state.[36] The nondissociated PCA molecule indeed demonstrated weaker binding to Au compared to the PSA anion (Figure S7i,j). These results explained the limited assembly of AuNPs observed on the graphitic surfaces with carboxylic functionalities. With no strong binding site, the adsorbed AuNPs were less likely to meet with each other before diffusing back to the solution phase, and thus no welding happened during this process.

The adsorbed AuNPs could diffuse on the surface of either CNTs or graphene (second step). We hypothesize a "shuttling mechanism" for this process considering the different results from SWNT-PSA/CCG-PSA and S-SWNTs/S-CCG. After AuNPs bind to the sulfonic groups, the diffusion of PSA molecules on the SWNTs/CCG could carry the AuNPs to assemble together. Due to the weak binding, however, this assembly process did not occur when carboxylic groups were the major surface functionalities. In the case of S-SWNTs and S-CCG, due to the covalent bonding on the surfaces, no "shuttling" of AuNPs would happen. Instead, the AuNPs tightly bound to the sulfonic groups probably acted as a welding center for other AuNPs. The intermediate level of AuNWs formation was a consequence of the competition between the diffusion of AuNPs on the template surface to meet bounded AuNPs and diffusion of AuNPs back to solution.

This diffusion step is illustrated in Figure 3l–n in which we present the minimum energy diffusion profiles of a Au_{20} cluster on a SWNT in an axial direction (Figure 3l) or on a graphene surface (Figure 3m,n) along the P1 and P2 directions shown in Figure 3o. For both cases, the barriers for diffusion were small, with values of ~1 kcal/mol. This result indicated that the role of "shuttling" molecules in the self-assembly of AuNPs was not to overcome the energy barriers of in-plane diffusion, which are negligible at room temperature conditions. Instead, the "shuttling" molecules provide stronger binding sites for AuNPs than those on pristine SWNTs (Figure 3e) or graphene (Figure 3g). Such an increased stability is necessary in order to keep the adsorbed AuNPs diffusing (SWNT-PSA/CCG-PSA) or staying attached (S-SWNTs/S-CCG) to the graphitic surface long enough to encounter other AuNPs instead of returning to the solution phase. A similar simulation also revealed that the in-plane diffusion of PSA had a small energy barrier (Figure S8a,b). It should also be noted that no obvious energy difference was found for diffusion barriers of AuNPs along different directions on the 2-D graphene (Figure 3m–o). Therefore, the diffusion of AuNPs on the graphitic templates was only confined by the dimensionality of the templates, and the resulting Au nanostructures after welding had the same dimensions as the templates (i.e., AuNWs formed on SWNT-

PSA or MWNT-PSA and Au plates formed on CCG-PSA). Another fact that should be pointed out was that AuNPs appeared to have a stronger interaction with graphene than SWNTs (Figure 3e,g); this could also explain why the aggregation level of AuNPs was higher on graphene templates than on SWNT templates (i.e., CCG-PCA vs SWNT-PCA, as shown in Figure 2b,f).

In the third step of the assembly and welding processes, AuNPs located in close proximity will fuse together. Such a process is illustrated in Figure 3k, where two Au_{20} clusters initially separated by 3.5 Å nanoweld simply due to the attractive nature of Au−Au interactions. Similar effects are depicted in Figure S8c,d for the welding of Au_{20} NPs on a graphene surface starting from different initial configurations. This welding process, achieved through coalescence of adjacent AuNPs, did not require high activation energy and could occur at temperatures much lower than the melting point. This is consistent with the examples of cold welding of Au nanomaterials without thermal heating that have been demonstrated in the literature.[17,37] Therefore, the thermal heating required in our method (Figure S9) was probably not for the activation of the welding process but rather for overcoming the electrostatic stabilization between individual AuNPs synthesized by citrate reduction.

It should also be noted that the three steps indicated above happen simultaneously in the aqueous system; in the first two steps, involving adsorption and NP diffusion, the individuality of AuNPs is maintained, while in the third step, upon welding, irreversible formation of AuNWs takes place.

Electrical Properties of AuNW-SWNTs. The current−voltage characteristics of AuNW-SWNT network was measured on a Keithley SourceMeter 2600, and the $I−V$ curves are shown in Figure S10. When this material is incorporated into an electrical circuit, both AuNWs and SWNTs conduct the electricity, and therefore, the Schottky barriers at AuNW−semiconducting SWNT junctions will contribute to the overall conductivity of the network. One practical advantage of such a combination is that these Schottky barriers are exquisitely sensitive to changes in the local chemical environment,[38,39] with direct applications in chemical sensing.

Hydrogen Sulfide (H_2S) Detection. The AuNW-SWNT sensor devices were fabricated by drop-casting the AuNW-SWNT suspension onto a Si chip with interdigitated gold electrodes; the size, pattern, and SEM images of a typical device are shown in Figure 4a−c. The H_2S response of AuNW-SWNTs was tested, and the data (Figure 4d,e) indicated that conductance of the AuNW-SWNT devices significantly decreased when they were exposed to H_2S at the concentration range from 10 ppb to 40 ppm (diluted in N_2). The detection of H_2S to 10 ppb in N_2 environment at room temperature meets the sensitivity requirement for a variety of applications ranging from mine safety to the detection of breath odor. The recommended exposure limit to H_2S is 10 ppm, and the presence of H_2S at 500 ppb (or higher) in human breath will cause halitosis (breath odor).[40,41] The cross-sensitivity of AuNW-SWNTs to other major components of natural gas (CH_4) and human breath (O_2, CO_2, H_2O, and artificial flavor compounds) was also tested, and no obvious cross-sensitivity was observed (Figure 4f,g). Although the H_2S response appeared to be irreversible at room temperature due to the well-known affinity of Au to S, the recovery of the baseline was achieved simply by heating the sensor chip at 140 °C for 30 min in ambient environment, and the sensor was found to be

reusable. Such heating induced recovery was also observed for other reported Au-based H$_2$S sensors.[21,23]

As a comparison, AuNP-SWNT devices fabricated by electrochemical deposition were also tested for their response to H$_2$S at both the ppb and ppm levels (Figure 4e). At the tested H$_2$S concentration ranges, AuNW-SWNTs appeared to have better sensitivity to H$_2$S, especially in the ppb level, with a detection limit for H$_2$S of ~1 order of magnitude lower than that of AuNP-SWNTs (the detection limit of AuNW-SWNTs was calculated to be 5 ppb, while the detection limit of AuNP-SWNTs was determined to be ~50 ppb, data shown in Figure S12). H$_2$S tests were also conducted on pristine SWNTs, and much smaller response was observed (Figure 4e).

The enhanced chemical sensitivity of AuNW-SWNTs is believed to result from a different sensing mechanism. The sensing mechanism of the AuNP-SWNTs system involves the H$_2$S-induced charge transfer from AuNPs to the SWNT network.[23] In the AuNW-SWNTs architecture, however, 1-D AuNWs can form several connections between SWNTs, and thus create additional electrical pathways through the SWNT network. Since the AuNWs become part of the conducting network, the adsorption of H$_2$S molecules could create scattering centers and modulate the Schottky barriers at the AuNW-SWNT interfaces, which would more effectively decrease the conductivity of the sensing network.

CONCLUSION

In summary, we have explored the self-assembly and nano-welding processes of AuNPs on graphitic templates and demonstrated a simple yet scalable bottom-up approach for the synthesis of 1-D AuNWs using AuNPs as building blocks. SWNTs-PSA appeared to be an effective template material for 1-D assembly of AuNPs, and subsequent nanowelding of aligned AuNPs could be induced by thermal heating to form 1-D AuNWs. DFT simulations elucidated the mechanism of this process. The three-step model revealed in this work, which included adsorption, in-plane diffusion ("shuttling"), and nanowelding, provided some insights into controlling and manipulating the motion of nanoparticles on the graphitic surface, and this work supplemented the existing toolbox of bottom-up fabrication techniques for complex material architectures. Additionally, the AuNW-SWNT network showed ultrasensitivity to H$_2$S in both the ppb and ppm levels with a detection limit as low as 5 ppb at room temperature. This hybrid material exhibited a promising potential for incorporation into a portable, low-power, inexpensive, and easy-to-use detection tool for applications such as industrial control, personal safety, or personal healthcare.

EXPERIMENTAL SECTION

Materials. Pristine single-walled carbon nanotubes (SWNTs, P2) and carboxylated single-walled carbon nanotubes (SWNT-COOH, P3) were obtained from Carbon Solutions Inc. 1-Pyrenesulfonic acid hydrate (1-PSA, C$_{16}$H$_{10}$O$_3$S·xH$_2$O), 1-pyrenecaboxylic acid (1-PCA, C$_{17}$H$_{10}$O$_2$, 97%), gold(III) chloride trihydrate (HAuCl$_4$·3H$_2$O, 99.9+% trace metals basis), sodium borohydride (NaBH$_4$), and all organic solvents were purchased from Sigma Aldrich and used as received. Sodium citrate dihydrate was acquired from Mallinckrodt Baker Inc., and 40 lead ceramic sidebraze (CERDIP) packages (cavity 0.310 × 0.310) were procured from Global Chip Materials, LLC.

Preparation of Different Graphitic Templates. *PSA/PCA-Functionalized SWNTs (SWNT-PSA/SWNT-PCA).*[26] SWNTs powder (5.0 mg) was sonicated in deionized (DI) water (10 mL) with a Branson 5510 bath sonicator for 15 min to obtain a temporary

SWNTs suspension. Aqueous solution of 1-PSA or methanol solution of 1-PCA (10 mL, 0.5 mg/mL) was added into this SWNTs suspension, following by sonication for 30 min. The resulting SWNT-PSA/SWNT-PCA complex was separated out by centrifugation and washed with DI water three times to afford the final product, which was resuspended in 20 mL of DI water.

Sulfonated SWNTs (S-SWNT). Pristine SWNTs were oxidized with nitic acid and sulfuric acid (1:3) following a reported procedure.[42] The oxidized SWNTs (5.5 mg) were then suspended in water (7.5 mL) and sulfonated with aryl diazonium salt of sulfanilic acid followed by a hydrazine reduction for 24 h, similar to a previous publication.[29] [**Caution** *should be taken when using hydrazine because it is extremely flammable and toxic.*] The final product was filtrated, washed with DI water three times, and finally suspended in 20 mL of DI water.

Graphene Oxide (GO) and Chemically Converted Graphene (CCG). Utilizing a modified Hummers' method, graphite oxide was prepared on graphite flakes that underwent a preoxidation step.[43] GO (~0.125 wt %) was subsequently formed from graphite oxide that was diluted 1:4 with doubly distilled water, exfoliated for 45 min by sonication, and centrifuged for 30 min at 3400 rpm to remove unexfoliated graphite oxide. To form CCG, GO was reduced following a modified procedure.[29] Briefly, the pH of a dispersion of GO (75 g) in water was adjusted to ~9 with sodium carbonate, and the GO dispersion was partially reduced through the addition of sodium borohydride (600 mg). After the partially reduced GO dispersion was heated at 80 °C for 1 h under constant stirring, the material underwent four sequential washing/centrifugation cycles, and the partially reduced GO was dispersed in water via mild sonication for a final mass of 75 g. Finally, the dispersion of partially reduced GO was reduced by hydrazine. To this end, 50 wt % hydrazine hydrate (4 g) was added to the dispersion of partially reduced GO, which was subsequently refluxed at 100 °C for 24 h under constant stirring. After refluxing, the CCG was subjected to four sequential washing/centrifugation cycles.

PSA- and PCA-Functionalized CCG (CCG-PSA and CCG-PCA). CCG-PSA and CCG-PCA were synthesized using the same method for the synthesis of SWNT-PSA and SWNT-PCA.

Sulfonated Chemically Converted Graphene (S-CCG). S-CCG was synthesized using the same method for the synthesis of S-SWNTs.

Self-Assembly and Nanowelding of Gold Nanoparticles. *Using SWNT-PSA Template: Synthesis of AuNW-SWNTs.* HAuCl$_4$ (0.5 mg) was dissolved in an aqueous suspension of PSA-functionalized SWNTs (19 mL, 0.025 mg/mL). An aqueous solution of sodium citrate (1 wt %, 1 mL) was then added into a HAuCl$_4$ and SWNT-PSA solution with vigorous stirring. The mixture solution was heated to 100 °C for 30−120 min to yield a purple suspension of SWNTs. The final product was isolated by centrifugation, washed with DI water several times, and then resuspended in 20 mL of DI water. Control experiments were done under similar conditions without the presence of CNTs in the solution.

Using Other Graphitic Template. Self-assembly and nanowelding processes on other graphitic templates (including SWNT-PCA, SWNT-COOH, S-SWNTs, GO, CCG-PSA, CCG-PCA, and S-CCG) were carried out with the same procedure used with the SWNT-PSA template.

Sensor Device Fabrication. Si chips with a 300 nm thermal oxide layer and interdigitated gold electrodes were purchased from MEMS and Nanotechnology Exchange. The devices were fabricated by drop-casting aqueous suspension (10 μL) of AuNW-SWNTs or DMF suspensions (70 μL) of SWNTs onto the Si chips which were connected to the 40 CERDIP Packages with Au wires and allowed to dry in ambient.

Gas Sensing Measurements. Gas sensing measurements were carried out using a custom-made system that has been described in our previous publications.[38,44] In particular, electrical conductance of two chips (with 8 data output) can be measured on a test board by Keithley Dual SourceMeter 2602 and Keithley Switching Matrix 708A, controlled by a Zephyr Measurement Software (http://zephyr.

sourceforge.net). A custom-built Teflon chamber was used to control the gas environment during the sensing test. Different concentrations of analyte gases were generated by mixing certified gases (100 ppm H_2S in N_2 or 1 ppm H_2S in N_2, purchased from Valley National Gas, Inc.) with dry N_2 and were passed through the gas chamber containing the sensor device.

■ ASSOCIATED CONTENT

Ⓢ Supporting Information

Experimental details for general material characterizations, spectroscopic characterizations and computational methods, TEM characterizations of control experiments, additional computational results, $I-V$ characteristics of AuNW-SWNTs and its response to humidity. This material is available free of charge via the Internet at http://pubs.acs.org.

■ AUTHOR INFORMATION

Corresponding Author
astar@pitt.edu

Notes
The authors declare no competing financial interest.

■ ACKNOWLEDGMENTS

■ REFERENCES

(1) Redl, F. X.; Cho, K. S.; Murray, C. B.; O'Brien, S. *Nature* **2007**, *423*, 968−971.

(2) Lu, W.; Lieber, C. M. *Nat. Mater.* **2007**, *6*, 841−850.

(3) Mann, S. *Nat. Mater.* **2009**, *8*, 781−792.

(4) Wang, C.; Hu, Y.; Lieber, C. M.; Sun, S. *J. Am. Chem. Soc.* **2008**, *130*, 8902−8903.

(5) Xiang, C. X.; Kim, J. Y.; Penner, R. M. *Nano Lett.* **2009**, *9*, 2133−2138.

(6) Zhang, X. P.; Sun, B. Q.; Hodgkiss, J. M.; Friend, R. H. *Adv. Mater.* **2008**, *20*, 4455−4459.

(7) Zhang, X. Y.; Li, D.; Bourgeois, L.; Wang, H. T.; Webley, P. A. *ChemPhysChem* **2009**, *10*, 436−441.

(8) Ofir, Y.; Samanta, B.; Rotello, V. M. *Chem. Soc. Rev.* **2008**, *37*, 1814−1825.

(9) Chen, C. L.; Rosi, N. L. *Angew. Chem., Int. Ed.* **2010**, *49*, 1924−1942.

(10) Halder, A.; Ravishankar, N. *Adv. Mater.* **2007**, *19*, 1854−1858.

(11) Feng, H. J.; Yang, Y.; You, Y.; Li, G.; Guo, J.; Yu, T.; Shen, Z.; Wu, T.; Xing, B. *Chem. Commun.* **2009**, 1984−1986.

(12) Kundu, P.; Halder, A.; Viswanath, B.; Kundu, D.; Ramanath, G.; Ravishankar, N. *J. Am. Chem. Soc.* **2010**, *132*, 20−21.

(13) Tang, Z.; Kotov, N. A.; Giersig, M. *Science* **2002**, *297*, 237−240.

(14) Koh, W. K.; Bartnik, A. C.; Wise, F. W.; Murray, C. B. *J. Am. Chem. Soc.* **2010**, *132*, 3909−3913.

(15) Kim, S. J.; Jang, D. J. *Appl. Phys. Lett.* **2005**, *86*, 033112.

(16) Peng, Y.; Cullis, T.; Inkson, B. *Nano Lett.* **2009**, *9*, 91−96.

(17) Lu, Y.; Huang, J. Y.; Wang, C.; Sun, S.; Lou, J. *Nat. Nanotech.* **2010**, *5*, 218−224.

(18) Huang, Y.; Chiang, C.; Lee, S. K.; Gao, Y.; Hu, E. L.; Yoreo, J. D.; Belcher, A. M. *Nano Lett.* **2005**, *5*, 1429−1434.

(19) McNerney, J. J.; Buseck, P. R.; Hanson, R. C. *Science* **1972**, *178*, 611−612.

(20) Yoo, K. S.; Sorensen, I. W.; Glaunsinger, W. S. *J. Vac. Sci. Technol. A* **1994**, *12*, 192−198.

(21) Geng, J.; Thomas, M. D. R.; Shephard, D. S.; Johnson, B. F. *Chem. Commun.* **2005**, 1895−1897.

(22) Penza, M.; Rossi, R.; Alvisi, M.; Cassano, G.; Serra, E. *Sens. Actuators B* **2009**, *140*, 176−184.

(23) Mubeen, S. A.; Zhang, T.; Chartuprayoon, N.; Rheem, Y.; Mulchandani, A.; Myung, N. V.; Deshusses, M. A. *Anal. Chem.* **2010**, *82*, 250−257.

(24) Kolmakov, A.; Moskovits, M. *Annu. Rev. Mater. Res.* **2004**, *34*, 151−180.

(25) Zhang, T.; Mubeen, S.; Myung, N. V.; Deshusses, M. A. *Nanotechnology* **2008**, *19*, 332001.

(26) Ding, M.; Tang, Y.; Gou, P.; Reber, M. J.; Star, A. *Adv. Mater.* **2011**, *23*, 536−540.

(27) Wu, Y.; Yang, P. *Adv. Mater.* **2001**, *13*, 520−523.

(28) Simmons, T. J.; Bult, J.; Hashim, D. P.; Linhardt, R. J.; Ajayan, P. M. *ACS Nano* **2009**, *3*, 865−870.

(29) Si, Y.; Samulski, E. T. *Nano Lett.* **2008**, *8*, 1679−1682.

(30) Dreyer, D. R.; Park, S.; Bielawski, C. W.; Ruoff, R. S. *Chem. Soc. Rev.* **2010**, *39*, 228−240.

(31) Sainsbury, T.; Stolarczyk, J.; Fitzmaurice, D. *J. Phys. Chem. B* **2005**, *109*, 16310−16325.

(32) Rance, G. A.; Marsh, D. H.; Bourne, S. J.; Reade, T. J.; Khlobystov, A. N. *ACS Nano* **2010**, *4*, 4920−4928.

(33) Diamanti, S.; Elsen, A.; Naik, R.; Vaia, R. *J. Phys. Chem. C* **2009**, *113*, 9993−9997.

(34) Heinz, H.; Farmer, B. L.; Pandey, R. B.; Slocik, J. M.; Patnaik, S. S.; Pachter, R.; Naik, R. R. *J. Am. Chem. Soc.* **2009**, *131*, 9704−9714.

(35) Sato, M.; Kaieda, T.; Ohmukai, K.; Kawazumi, H.; Ogawa, T. *Anal. Sci.* **1998**, *14*, 855−856.

(36) Zelent, B.; Vanderkooi, J. M.; Coleman, R. G.; Gryczynski, I.; Gryczynski, Z. *Biophys. J.* **2006**, *91*, 3864−3871.

(37) Ferguson, G. S.; Chaudhury, M. K.; Sigal, G. B.; Whitesides, G. M. *Science* **1991**, *253*, 776−778.

(38) Kauffman, D. R.; Star, A. *Nano Lett.* **2007**, *7*, 1863−1868.

(39) Kauffman, D. R.; Sorescu, D. C.; Schofield, D. P.; Allen, B. L.; Jordan, K. D.; Star, A. *Nano Lett.* **2010**, *10*, 958−963.

(40) Suarez, F. L.; Furne, J. K.; Springfield, J.; Levitt, M. D. *J. Dent. Res* **2000**, *79*, 1773−1777.

(41) Tangerman, A.; Winkel, E. G. *J. Breath Res.* **2010**, *4*, 017003.

(42) Liu, J.; Rinzler, A. G.; Dai, H.; Hafner, J. H.; Bradley, R. K.; Boul, P. J.; Lu, A.; Iverson, T.; Shelimov, K.; Huffman, C. B.; Rodriguez-Macias, F.; Shon, Y.; Lee, T. R.; Colbert, D. T.; Smalley, R. E. *Science* **1998**, *280*, 1253−1256.

(43) Kovtyukhova, N. I.; Ollivier, P. J.; Martin, B. R.; Mallouk, T. E.; Chizhik, S. A.; Buzaneva, E. V.; Gorchinskiy, A. D. *Chem. Mater.* **1999**, *11*, 771−778.

(44) Star, A.; Joshi, V.; Skarupo, S.; Thomas, D.; Gabriel, J.-C. P. *J. Phys. Chem. B* **2006**, *110*, 21014−21020.